Structure, Vol. 13, 1789–1798, December, 2005, ©2005 Elsevier Ltd All rights reserved. DOI 10.1016/j.str.2005.08.022

How pH Opens a H^+ Channel: The Gating Mechanism of Influenza A M2

Itamar Kass[1] and Isaiah T. Arkin[1,*]
[1] Department of Biological Chemistry
The Alexander Silberman Institute of Life Sciences
The Hebrew University of Jerusalem
Edmond J. Safra Campus
Givat-Ram
Jerusalem, 91904
Israel

Summary

The tetrameric M2 protein from influenza A is one of the simplest pH-gated H^+ channels known, offering the potential of structurally characterizing its gating mechanism. Since the only ionizable groups in the pore are four histidines, we investigated the stability and dynamics of all six possible protonation states of the protein by using molecular dynamics. We show that while all channel protonation states are surprisingly stable, only systems with two or more charged histidines are appreciably conductive. The structural switch, from a uniprotonated to a biprotonated channel, causes an electrostatic repulsion between the charged histidines that pushes the helices apart. This results in the formation of a continuous water file that conducts protons via a H^+ wire. pKa calculations place this transition at a pH of 5.6, in remarkable agreement with the experimental value. Since the conversion from uniprotonation to biprotonation occurs during endosome acidification, this explains how M2 is activated in vivo.

Introduction

The influenza virus is the causative agent of one of the most taxing of all infectious diseases. A critical component of the virus is the M2 protein, which plays a vital role in the viral entry process via endocytotic uptake. M2 is activated in the acidifying endosome, allowing protons to pass into the virus interior (Pinto et al., 1992). The resulting acidification of the virus lumen releases the viral RNA genome from its matrix, enabling it to diffuse into the cytoplasm after viral membrane fusion. The pivotal role of M2 in viral replication is further exemplified by the fact that amino-adamantanes that block its H^+ channel activity make potent anti-influenza agents (Hay et al., 1985; Pinto et al., 1992).

Functionally, the activation of the M2 channel is believed to happen in response to an outer pH drop. Due to activation, protons are selectively transported across the viral membrane (Chizhmakov et al., 1996). The extent of conductivity of M2 was recently shown to be as high as 6 pS, leading to measured H^+ currents of up to 0.7 pA (Vijayvergiya et al., 2004). This value is higher by several orders of magnitude than earlier subfemto-Siemens estimates (Lin and Schroeder, 2001), and, as such, earlier analyses of M2 conductivity require revision in light of the new results.

The mechanism of M2's proton conductivity and pH activation is a matter of debate as well. Two main conductivity mechanisms were suggested: gating (Sansom et al., 1997) and shuttling (Sakaguchi et al., 1997). In the gating mechanism, conductivity is achieved when water molecules are able to penetrate the channel throughout, forming a continuous, conductive proton wire (Brewer et al., 2001). In the slower shuttling mechanism, the histidines are directly involved in the proton transfer mechanism. A biprotonated histidine intermediate is transiently formed, leading to rapid proton release at the opposite side of the histidine ring. Regeneration occurs through tautomerization or flipping of the imidazole ring. A detailed kinetic analysis of the shuttling mechanism was suggested by Lear (2003), prior to the advent of new conductivity data (Vijayvergiya et al., 2004).

Structurally, M2 is a 96 amino acid, homotetrameric protein, whereby tetramerization, H^+ conductivity, and amantadine binding are functions of its single α-helical (Duff et al., 1992) transmembrane domain (Sugrue and Hay, 1991; Pinto et al., 1992, 1997; Holsinger et al., 1995; Duff and Ashley, 1992). Detailed structural analyses of the transmembrane domain of M2 have been carried out by using solid-state NMR (Kovacs and Cross, 1997; Kovacs et al., 2000; Song et al., 2000; Wang et al., 2001; Nishimura et al., 2002) and isotope-edited site-specific FTIR (Kukol et al., 1999; Torres et al., 2000, 2001; Torres and Arkin, 2002). The tilt angle of the helices from the membrane normal was shown to be 32°–38° both by NMR (Kovacs and Cross, 1997) and by site-specific FTIR (Kukol et al., 1999). Both of the above-described studies were also able to derive the rotational positioning of the helices with respect to each other, leading to molecular models for the protein. The models place the histidine residues implicated in channel activation (Wang et al., 1995) in the pore lining, as expected. Finally, a series of peptides, each containing a single ^{15}N-labeled amino acid, was used to measure the anisotropic ^{15}N-^{1}H dipolar and ^{15}N chemical shift interactions by solid-state NMR (Kovacs et al., 2000). This led to a detailed structure of the peptide protomer. Molecular modeling aided by a single intermolecular distance restraint was then used to form the tetrameric structure giving rise to a model of the closed state of the transmembrane domain of M2 (Nishimura et al., 2002).

In a tetrameric channel with four histidine residues, there are six different potential protonation states, as shown in Figure 1. Clearly, knowledge of which of the six different protonation states are present natively in the channel is essential to the understanding of the exact proton transfer mechanism. Experimentally, using UV Raman spectroscopy of M2 in lipid bilayers, Takeuchi and coworkers have measured the pKa of the histidine residues to be 5.77 ± 0.06 (Okada et al., 2001; Takeuchi et al., 2003). This value agrees well with the pH required to activate the channel (Wang et al., 1995), indicating that it is a protonation change of the histidine residues that is responsible for channel gating.

*Correspondence: arkin@cc.huji.ac.il

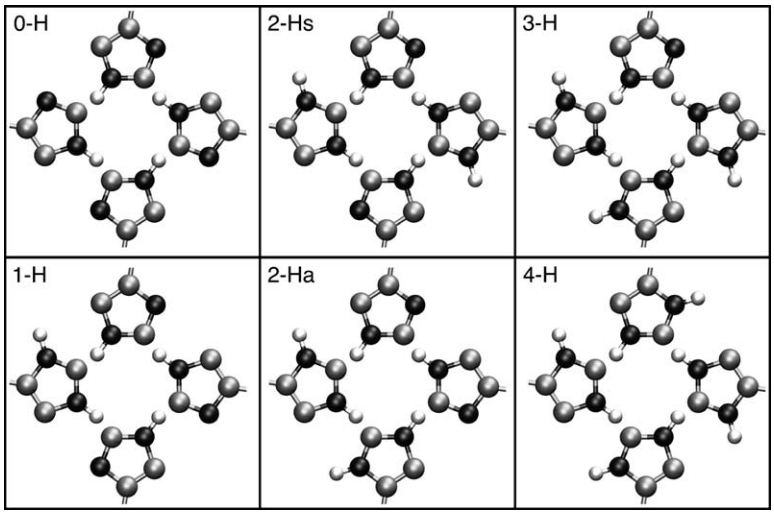

Figure 1. M2 Protonation Configurations

A schematic 2D representation of the six possible protonation states of the four histidine residues of the influenza A M2 H^+ channel tetrameric complex. The respective positions of the histidine residues are not based on the SS-NMR (Nishimura et al., 2002) or MD structural model. 2-Hs and 2-Ha are the complexes with two biprotonated histidine residues in symmetric and asymmetric configurations, respectively.

Due to its small size and pharmaceutical importance, M2 has been a target of several modeling exercises (Pinto et al., 1997; Sansom et al., 1997; Kim et al., 2003). Prior to any structural analyses of M2, models for the complex were proposed based on molecular dynamics (MD) simulations by the groups of DeGrado and Sansom (Pinto et al., 1997; Sansom et al., 1997). Both models resemble the structures from NMR (Nishimura et al., 2002) and FTIR (Kukol et al., 1999) regarding the rotational positioning of the helices, which place the histidine residues facing the pore. Yet, major differences are seen in the helix tilt angles between the experimental and computational models. The theoretical models predicted helix tilt angles of 10°–15°, a range much lower than that determined experimentally: 32°–38° (Kovacs and Cross, 1997; Kukol et al., 1999). The low tilt angles may have been due to the fact that in these studies, modeling of the M2 complex was done in vacuo and included artificial interhelix distance restraints to maintain bundle integrity. Although in vacuo simulations are much faster than simulations done in an explicit membrane model, they are limited in that they do not include the phospholipid bilayer and water environment. Simulations of the M2 complex within an octane slab have overcome this problem to an extent (Zhong et al., 1998, 2000). More realistic simulations, in which the M2 tetrameric complex was solvated in a lipid bilayer, were conducted (amongst others) in diphytanol phosphocholine (Husslein et al., 1998) or hydrated 1-palmitoyl-2-oleoyl-sn-glycerol-3-phosphocholine (Forrest et al., 2000; Sansom et al., 1998).

A different simulation was conducted by Voth and coworkers in which the proton conductance was investigated in the M2 complex solvated in dimyristoylphosphocholine and water (Smondyrev and Voth, 2002). The study focused on a system consisting of one biprotonated histidine residue (1-H, see Figure 1). Based on the data, which were collected by using MD combined with a multistate empirical valence bond approach (Schmitt and Voth, 1998, 1999a, 1999b), the passage of a proton through the channel (via the gating mechanism) may be accompanied by concerted changes of the channel conformation.

However, none of the above-described simulations (in vacuum, octane slab, or lipids) were based on the recent experimentally derived structure of M2 by solid-state NMR (Nishimura et al., 2002). Moreover, none of the above-described studies have simulated all possible protonation states of the channel. Thus, we decided to investigate the activation and conductivity of the M2 channel in detail, by using long molecular dynamics simulations in a fully hydrated lipid bilayer starting from the experimentally determined structure of the protein. We focused on determining the conductive properties of all possible histidine protonation states of the channel, as it is key in the channel gating process.

Results

Overview

Molecular dynamics simulations provide a powerful tool by which to analyze the conductivity and selectivity of membrane proteins. For example, studies from the groups of Roux, Schulten, Grubmuller, and Sansom (to name a few) were able to gain insight into the conductivity mechanisms of K^+ (Noskov et al., 2004) and water channels (de Groot and Grubmuller, 2001; Tajkhorshid et al., 2002). Similarly, in the current study, we wished to examine the gating behavior of M2 by embedding the experimentally determined structure of the transmembrane domain of M2 (Nishimura et al., 2002) in a lipid bilayer composed of 128 dimyristoylphosphocholine lipid molecules. The entire bilayer was then solvated by 3687 water molecules with an appropriate number of Na^+ cations to neutralize the system charge (Figure 2). The protonation state of His37 was adjusted in order to simulate each of the six different protonation states of the complex (see Figure 1). After system relaxation, a molecular dynamics trajectory was conducted for each system for a period of 7.5 ns in order to investigate the properties of the system.

Membrane Stability during the Simulation

In order to assess the behavior and normality of the entire system during the simulation, the atomic densities of the lipid head groups were calculated as a measure of

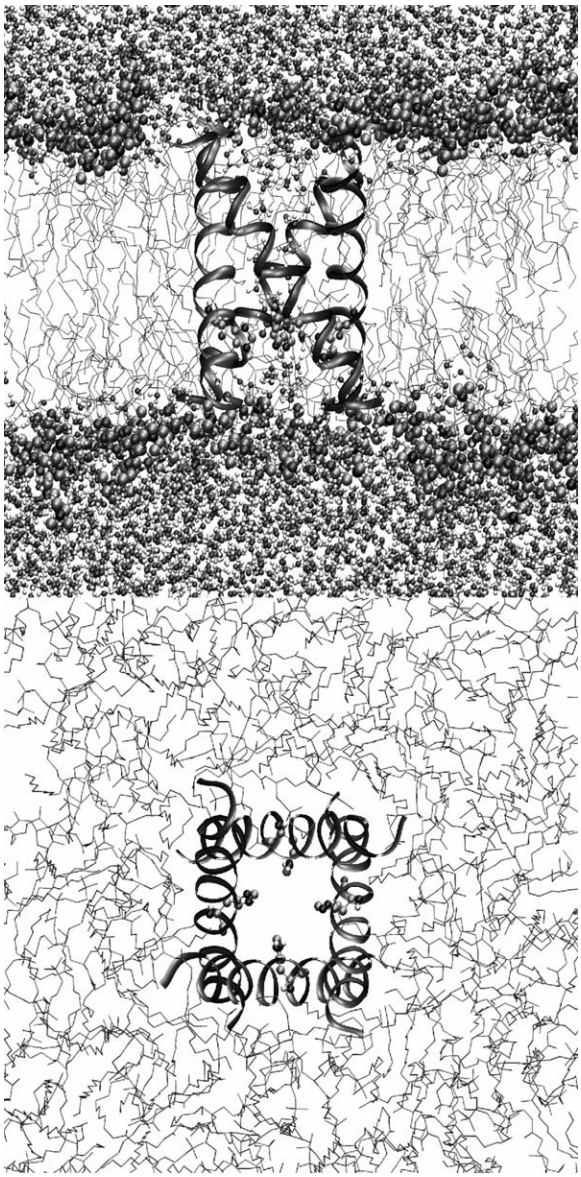

Figure 2. M2 Simulation System

Top panel: side view of the starting configuration of the simulation system for the M2 complex. The histidine ring is shown in CPK representation. Bottom panel: top view of the starting configuration of the simulation. This figure was drawn with the program VMD (Humphrey et al., 1996) and was rendered in PovRay 3.6 (Persistence of Vision Raytracer Pty. Ltd., 2004).

bilayer mean thickness. The distance between the head groups, 34.6 ± 2 Å, is in excellent agreement with recent experimental values reported from X-ray scattering (Arbely et al., 2004) of the M2 transmembrane peptide in dimyristoylphosphocholine membranes (see below). Thus, the thickness of the lipid bilayer containing the M2 protein in the simulation is virtually identical to that determined experimentally for the same system.

Channel Stability

In order to compare the relative stabilities of the different protonation states within the dimyristoylphosphocholine bilayer, the root-mean-square deviations of the protein's Cα atoms (Cα-rmsd) relative to the initial structure were calculated over the time course of the simulation. As seen in Figure 3, all six protonation systems show an increase in the Cα-rmsds at the very beginning (first 100 ps), after which the Cα-rmsd values gradually increase until stable states are archived. Plateau Cα-rmsd values, between 2.5 Å and 4 Å, are achieved at the productive state of the simulation (in the last 4.5 ns).

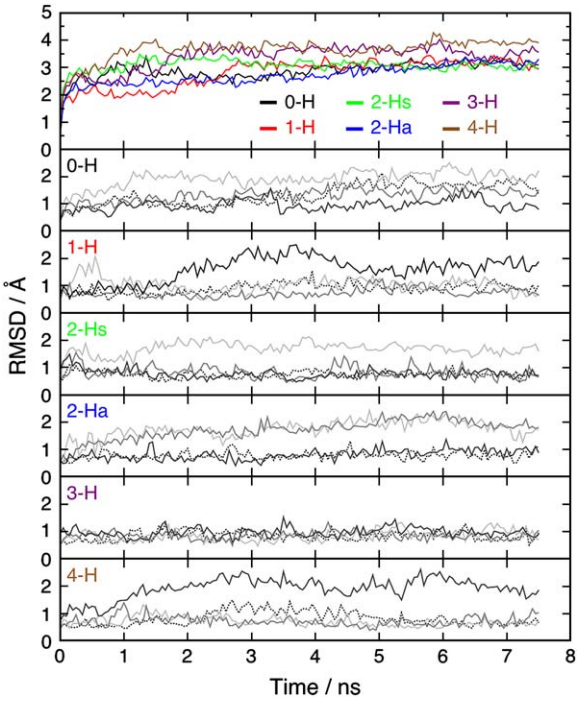

Figure 3. Cα-Rmsd Analysis of M2 Complexes during the 7.5 ns Simulation

The top panel represents the Cα-rmsd of the entire tetrameric complex from the solid-state NMR structure (Nishimura et al., 2002) for each of the individual protonation systems as indicated. Black, 0-H; red, 1-H; green, 2-Hs; blue, 2-Ha; purple, 3-H; brown, 4-H (see Figure 1). The lower six panels depict the Cα-rmsd of each of the individual helices from the solid-state NMR structure (Nishimura et al., 2002). Each panel lists the results for the individual systems as indicated.

The Cα-rmsd values indicate that, while some structural rearrangement does occur, a stable structure is achieved for all six of the systems regardless of the protonation state. The largest structural rearrangements relative to the initial configurations are seen in protonation systems 3-H and 4-H. This is probably due to electrostatic repulsion between the charged histidine residues, which are not present in the solid-state NMR model that was constructed with neutral histidines only (Nishimura et al., 2002).

In analyzing the magnitude of the Cα-rmsd changes from the initial structure, it is important to note that aside from a single interhelical distance restraint (Nishimura et al., 2002), all other data provided by solid-state NMR studies pertain only to the protomer structure. In other words, the orientational restraints obtained by the ^{15}N NMR do not provide any structural restraints that relate the helices to one another. Construction of

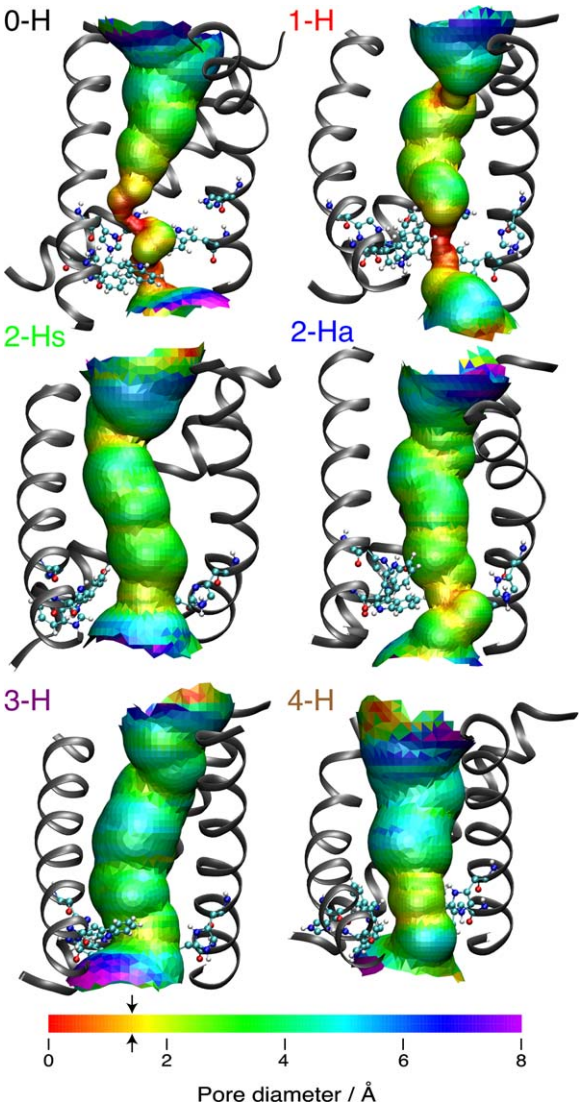

Figure 4. Pore Diameters as a Function of the Channel Protonation State

Representation of the pore size of the time average structure (over the simulation's productive state) of the different M2 systems. His37 and Trp41 are shown in wire frame. One of the four helices is removed for clarity. The color coding is according to the legend at the bottom. The arrows in the color legend represent the radius of a water molecule at 1.41 Å. The calculation of pore radii was done with the program HOLE (Smart et al., 1996). This figure was drawn with the program VMD (Humphrey et al., 1996) and was rendered in PovRay 3.6 (Persistence of Vision Raytracer Pty. Ltd., 2004).

the tetrameric structure was done by in vacuo molecular modeling, taking into account the single interhelical distance between $^{15}N_{\pi}$ and $^{13}C_{\gamma}$ (Nishimura et al., 2002). It is for this reason that much lower Cα-rmsd values are observed when comparing the individual helices during the dynamics trajectory to the initial model (Figure 3, lower panels). Moreover, the structure derived from the solid-state NMR is explicitly that of the closed form of the channel (Nishimura et al., 2002). Furthermore, any differences between the structures seen in the simulation may reflect the experimentally measured inherent plasticity of the protein (Duong-Ly et al., 2005).

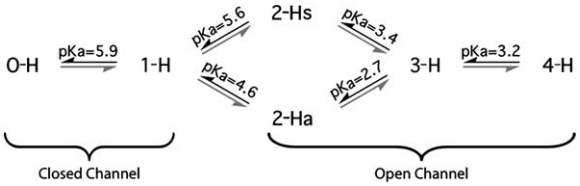

Figure 5. pKa Transitions of the Protonation Reaction in the M2 Channel

The pKa values for the different deprotonation reactions (black arrows) as calculated by using MEAD (Bashford and Gerwert, 1992). The corresponding protonation arrows are shown in gray.

Nevertheless, during simulation, there are structures in which the distance between $^{15}N_{\pi}$ and $^{13}C_{\gamma}$ is less than 3.9 Å, as measured by solid-state NMR (Nishimura et al., 2002).

Pore Profile Analysis

After establishing that the channel is stable regardless of its protonation states, we determined the effects of the histidine protonation state on the channel structure. In particular, we examined the pore radius of the average structure obtained during the productive state of the simulation for each of the six systems. As shown in Figure 4, there are significant differences between the pore radii of the different systems in the area of the histidine ring. The smallest minimal radii, 0.65 and 0.94 Å, are found for systems 0-H and 1-H, respectively, in the vicinity of His37. In contrast, the radii of systems 2-Hs, 2-Ha, 3-H, and 4-H, in the same location, are 2.7, 1.9, 2.9, and 2.6 Å, respectively.

Since the van der Waals radius of a water molecule is 1.41 Å, it is possible to conclude based on the protein structure alone that water cannot permeate the channel unless it contains two or more biprotonated histidine residues.

Channel Water Content

We next examined the potential conductivity of the channel by analyzing the water content in the pore directly. Water density profiles in the channel were calculated for the average structure of each protonation system. The results, shown in Figure 5, clearly indicate that, in systems with one or less charged histidines (i.e., 0-H and 1-H), there are several regions in the middle of the channel that are devoid of water. In such systems, H^+ conductivity would only be possible by employing the slow shuttling mechanism (Sakaguchi et al., 1997) (Figure 6). In contrast, in a channel with two or more biprotonated histidines, water is present throughout the pore. In such systems, a continuous water file is formed, facilitating the rapid passage of protons as a H^+ wire, with transient formation of Eigen or Zundel cations (Smondyrev and Voth, 2002).

pKa Calculation

The pKa values of the histidine residues, in the different protonation states, are strongly connected to the functionality of the M2 H^+ channel. Thus, knowledge of the pKa values is important for estimating the pH range in which a change in the histidine protonation state might occur. Toward this end, we carried out pKa calculations by using the program MEAD (Bashford and Gerwert,

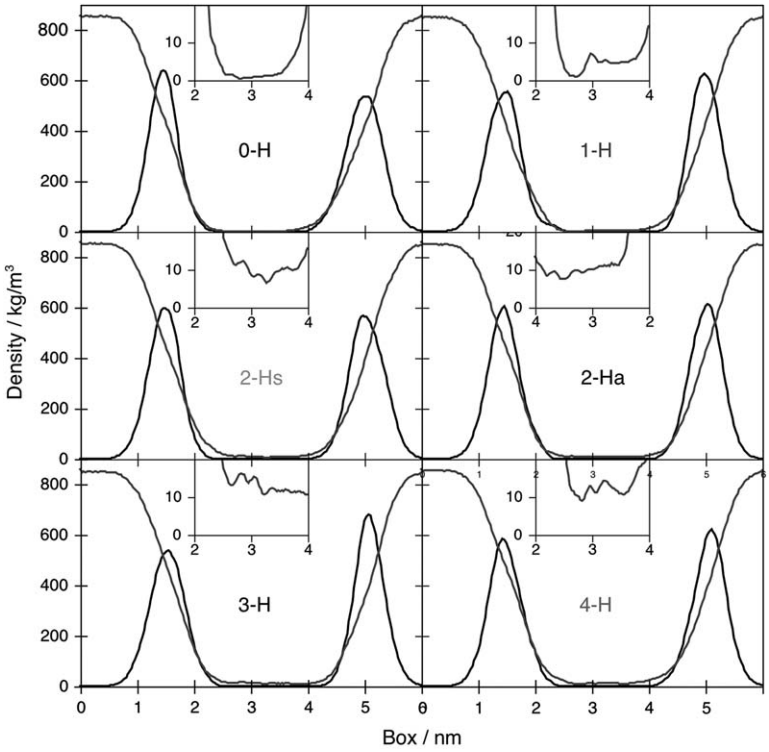

Figure 6. Representation of the Atomic Densities of Water and Lipid Head Groups for the Six Systems

Water densities are shown in gray, and lipid head groups are shown in black. The inset represents the density of water molecules in the center of the channel on an expanded scale.

1992), which calculated the pKa of the transition between different protonations by solving the Poisson-Boltzmann equation on a grid (Warwicker and Watson, 1982).

Initially, protonation calculations (aside from the 3-H → 4-H transition) revealed unrealistic values when deriving the pKas of the transitions that involve taking up a H^+ from solution. Since the structure of the protein remains static during the calculation, it was possible to deduce that the structure of the complex is incompatible with additional protonation steps. Thus, protonation most likely involves a conformational change in the protein to accommodate the excess charge.

Consequently, we have carried out the reverse pKa calculations for all of the deprotonation transitions, the results of which are shown in Figure 7. Two main trends were observed: (1) all resulting pKas of the histidine side chains were lower compared to an isolated imidazole group (pKa = 6.7). This is expected, since the histidine residues are located in a medium (the DMPC membrane) with a lower dielectric constant relative to water. (2) The valency of the transition is inversely correlated to the pH at which the transition takes place (aside from the 3-H → 4-H transition). In other words, the pKa of the 1-H → 2-H transition is higher than that of the 3-H → 4-H transition, but it is lower than that of the 0-H → 1-H transition. This is expected due to the fact that deprotonation is driven by electrostatic repulsion that takes place between multiple charged histidines.

Discussion

The purpose of this study was to investigate the effects of the histidine protonation state of the M2 channel on its structure and corresponding conductivity. Six different long molecular dynamics simulations were conducted of the M2 transmembrane domain embedded in a hydrated lipid bilayer. Each simulation was distinguished by its histidine protonation state and was based on the experimentally determined structure of the protein by solid-state NMR (Nishimura et al., 2002). To reiterate, the factors that distinguish this study from all previous simulations of M2 are: (1) a simulation based on the experimentally determined structure; (2) an analysis of all possible protonation states; and (3) a long, multinanosecond trajectory that allowed the simulations to reach equilibria.

Histidine Protonation Effect on Channel Structure

As suggested initially by Sansom and coworkers (Sansom et al., 1997) and Lear and coworkers (Zhong et al., 2000), the M2 channel may undergo a structural change upon altering its protonation state. Here, in a systematic analysis of all possible channel protonation states, to our knowledge, it is possible for the first time to place the change in channel structure precisely at the juncture between a uniprotonated and a biprotonated channel (see Figure 4).

The structural reasoning behind the change in channel structure is simple. In a system in which only one (or no) histidine is positively charged, there is no electrostatic repulsion to pry the ring of histidines open. The addition of another H^+ to the system results in electrostatic repulsion that takes place between two charged histidines. It is this Coulombic force that drives the histidines apart while they still face the channel's pore and enlarges the distance between the charged side chains. The withdrawal of the side chains from one another allows water molecules to permeate the channel throughout, as shown in Figure 6.

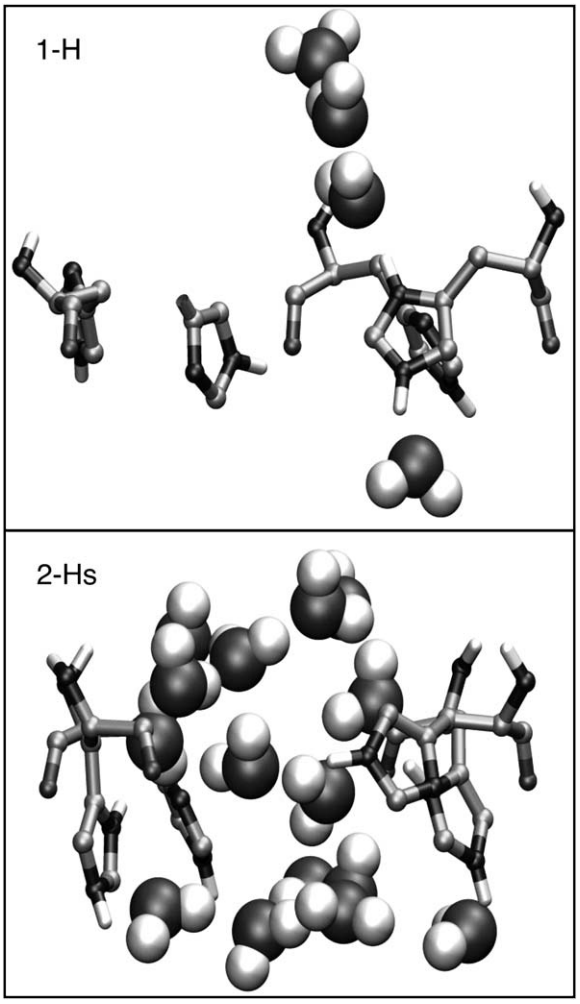

Figure 7. Structure of Two M2 Systems, 1-H and 2-Hs, in the Region of the Histidine Ring

Note the formation and lack thereof of the continuous water file in the system with two or one biprotonated histidines, respectively. The viewing direction in both panels is the same as that in the top panel of Figure 2. This figure was drawn with the program VMD (Humphrey et al., 1996) and was rendered in PovRay 3.6 (Persistence of Vision Raytracer Pty. Ltd., 2004).

The pore rearrangement as a function of the channel protonation state was evidenced by calculations of pKa values of the various transitions. Specifically, it was not possible to calculate pKa values for any channel protonation transition (aside from the 3-H → 4-H transition). Thus, it is possible to state that the channel must adopt its structure so as to enable further protonation. In other words, protonation events change the channel structure, as seen pictorially in Figure 4.

The values of the different protonation transitions could then be derived from the reverse deprotonation calculations (Figure 7). The values obtained are consistent with the fact that a transition from a uniprotonated system to a biprotonated system should take place at a lower pH than the transition from a neutral system to a uniprotonated system. Taken together, the pKa calculations enable us to place the activation of the channel, which occurs as the transition from a uniprotonated system to a biprotonated system, at a pH of 5.6 (Figure 7). This pH range is exactly that which is found in the endosome and explains how M2 is activated in the acidifying endosome (see below).

Interestingly, in contrast to previous assumptions (Zhong et al., 2000), the channel is stable regardless of its protonation state. Instabilities in prior studies could have been a result of a short simulation in an octane slab rather than a long simulation in a lipid bilayer. Moreover, increasing the protonation state of the channel beyond two biprotonated histidines does not result in substantial further opening of the channel (see Figure 4, panels for 2-Hs and 2-Ha versus those for 3-H and 4-H). Thus, to our knowledge, for the first time, we can place the switch the channel undergoes precisely at the juncture between a system containing one versus two biprotonated histidine residues. This is in contrast to a view of the channel as a faucet in which the number of protonated histidines correlates linearly with the channel pore diameter.

Conductivity Mechanism

The two conductivity mechanisms suggested for M2, gating (Sansom et al., 1997) and shuttling (Sakaguchi et al., 1997), may now be explained in molecular detail. We propose that shuttling is the only possible mechanism in a channel with less than two biprotonated histidines, while the faster gating mechanism will prevail in a channel with two or more biprotonated histidines. In systems with less than two charged histidines, water cannot support the formation of a continuous H^+ wire, since it does not permeate the channel throughout. In such systems, the only possible conductivity mechanism involves the direct shuttling of protons by an imidazole ring flip in the histidine constriction ring, as seen in Figure 8.

The maximal rate of conductivity via the shuttling mechanism is probably too low to account for the conductivity of the channel after activation. Specifically, H^+ currents of up to 0.7 pA (Vijayvergiya et al., 2004) would involve H^+ fluxes of 4.4×10^6 ions/s. This is several times faster than even the most rapid histidine-mediated H^+ shuttle known to take place in systems such as carbonic anhydrase (Lindskog, 1997). Thus, the shuttling mechanism might explain the basal conductivity of the protein in neutral conditions, prior to pH activation.

Upon protonation of a second histidine, electrostatic repulsion pries open the histidine constriction ring, supporting the formation of a continuous water file throughout the channel (Figure 4). Such a water file could conduct protons via a H^+ wire at rates that can readily account for the 0.7 pA current detected (Vijayvergiya et al., 2004).

In Vivo Channel Gating

Based on the above-described results, we propose the following scenario regarding the activation of the M2 channel in vivo: under neutral pH conditions prior to endocytic uptake, the channel is most likely neutral and lacks protonated histidines. Viral internalization by receptor-mediated endocytosis would lead to an increase in the number of biprotonated histidine residues, due to endosome acidification. The change to a channel with two or more positive charges would result in the creation of a continuous water file through the pore, supporting the formation of a proton wire. It is this proton

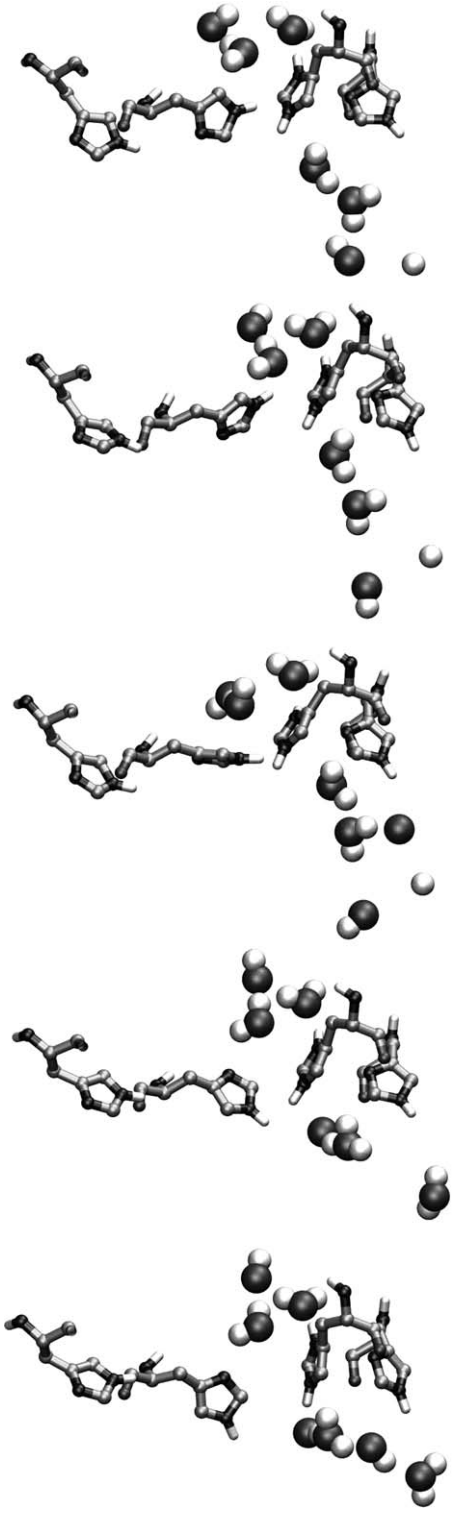

Figure 8. Histidine Ring Flipping

A sequence of structures of the histidine ring in a system with one biprotonated histidine showing an imidazole ring flip as a basis for the shuttling mechanism of proton conductivity. This figure was drawn with the program VMD (Humphrey et al., 1996) and was rendered in PovRay 3.6 (Persistence of Vision Raytracer Pty. Ltd., 2004).

wire that facilitates the marked proton conductivity that is seen experimentally as channel activation in low pH (Chizhmakov et al., 2003). Moreover, the pKa difference between the uniprotonated and biprotonated system is very small (Figure 7), leading us to speculate that the channel shifts rapidly from a neutral closed form to an open channel with two charged histidines, while the uniprotonated channel is only a short-lived intermediate. Finally, the pKa transition values indicate that, under normal conditions, the channel does not undergo any protonation beyond a biprotonated system. Therefore, the channel essentially has two states: a neutral closed state and a biprotonated open state. The neutral closed state predominates at neutral pH, while the open biprotonated state is that which is found in the acidified endosome.

That the channel has essentially only two states, neutral and a biprotonated species, is further strengthened by UV-Raman experiments (Okada et al., 2001; Takeuchi et al., 2003). The sigmoidal nature of the titration pKa profile (pD 4–9) of the histidine measured by Takeuchi and coworkers indicates that only a single transition takes place, at a pH of 5.8. This is exactly what we would expect from our pKa calculations. The only transition that we should observe in this pH range would be the transition for a neutral complex to a biprotonated system. This is due to the fact that the protonation of the neutral system to a uniprotonated complex occurs roughly at the same pH as the subsequent protonation step to a doubly charged system (see Figure 7).

In their experiments, Takeuchi and coworkers have shown that no change in the Raman signature of histidine at 1407 cm^{-1} is seen upon dissolving the membranes in SDS micelles at a pD of 4.0 below the measured pKa of 5.8 of the residues (Okada et al., 2001, Takeuchi et al., 2003). This is interpreted by the authors as evidence of the fact that all four histidine residues are biprotonated under native conditions. However, our calculations show that the pKas of all protonation reactions beyond a biprotonated system are below 4.0. Thus, at this pH, what the authors have seen is not the fully protonated system, but rather the doubly charged complex. We would predict that extending the measurements to lower pH values would lead to the identification of additional protonation events that are, however, of little biological relevance.

Histidine Presence in Ion Channels

The presence of histidines in ion channels and their influence on pH sensitivity points to the fact that the gating model described above may be applicable to proteins other than influenza A M2. For example, pH sensitivity involving histidine residues has been documented in a number of K^+ channels, such as ROMK1 (Chanchevalap et al., 2000), K_{ATP} (Xu et al., 2001), and Kv1.4 (Padanilam et al., 2002). Similarly, BM2, the influenza B M2 counterpart, has been shown to posses a histidine residue in the same location in its tetrameric complex (Mould et al., 2003). Finally, as a measure of the wide-spread presence of histidines in transmembrane domains of ion channels, a representative list of such proteins that we have compiled from the Swiss-Prot database is presented in Table 1.

Experimental Procedures

Initial Protein Structure

The initial M2 complex model is based on the bundle structure from solid-state NMR, PDB entry 1NYJ (Nishimura et al., 2002). During the

Table 1. Examples of Ion Channels that Contain Histidines in Their Transmembrane Domains

Protein Name	Transmembrane Domain
Cacophony protein Ca^{2+} channel (P91645)	WFYWFVIVLVFLNTVCVAVEHYG (441–463)
R-type Ca^{2+} channel (Q15878)	WLTHLLYYAEFLFLGLFLLEMSL (502–524)
ClC-0 Cl^- channel protein (P35522)	WFIPHLNIFIVMALYFVMHFWMA (381–403)
ClC-K1 Cl^- channel protein (Q06393)	WHFLVALGVLMALISYAMNFAIG (49–71)
ClC-K2 Cl^- channel protein (P51802)	WRGFFAATCGAFMFHLLAVF (236–255)
Na^+ channel protein type V (P15389)	WHMMDFFHAFLIIFRILC (881–898)
Paralytic protein Na^+ channel (P35500)	WNFTDFMHSFMIVFRVLC (980–997)
TASK-1 acid-sensitive K^+ channel (O14649)	WRFAGSFYFAITVITTIGYGHAA (77–99)
K^+ channel subfamily K member 7 (Q9Y2U2)	WSRYGLLVVAHLLALGLGAVVFQ (6–28)
TASK-5 acid-sensitive K^+ channel (Q8R5I0)	WRFAGSFYFAITVITTIGYGHAA (77–99)
ClC-1 Cl^- channel protein (P35523)	WIHPRVNVVIIIFLFFVM (448–465)
ClC-5 Cl^- channel protein (P51795)	WHLFELVPFILLGIFGGLWGALF (313–335)
K^+/Na^+ HCN1 channel (O60741)	WITMLSMIVGATCYAMFVGHATA (372-394)
Ork1 K^+ channel protein (Q94526)	WTFYHAFFFAFTVCSTVGYGNIS (89–111)
Acid-activated urea channel (P56874)	WYSLFVAINTVPAAILSHYS (105–124)
Aquaporin-CHIP (P29972)	HWIFWVGPFIGGALAVLIYDFIL (208–230)
L-type Ca^{2+} channel (Q13936)	HILFYFDIVFTTIFTIEIALKIL (930–952)
R-type Ca^{2+} channel (P56699)	HAFYWIVLGLVALNTVCVAVVHY (489–511)
L-type Ca^{2+} channel (O42398)	HVSDILNVAFTVLFTLEMILKLM (87–109)
Probable Ca^{2+} channel protein (P50077)	HYWFHNIKGFFLLVIFLFII (1617–1636)
Cyclic nucleotide-gated ion channel (Q9SU64)	HIFLITCLLALFLDPLYFYLPIV (56–78)
GEF1 protein (P37020)	HVSPFIIFMLLSVLFALISTLLV (153–175)
Glutamate receptor 3.1 precursor (Q7XJL2)	HSFWGMFLVVGIACLVALFIHFF (825–847)
GIRK1 K^+ channel (P48549)	HVGNYTPCVANVYNFPSAFLFFI (115–137)
Inward rectifier K^+ channel 4 (P52189)	HVNGFLGAFLFSVETQTTIGYGF (115–137)
Open rectifier K^+ channel protein 1 (Q94526)	HYVPPQLGLITTVVIALIPGIAL (164–186)
Probable aquaporin TIP type (P42067)	HVNPAVFGAFVGGNITLLRGIVY (82–104)
Probable aquaporin TIP type (P42067)	HWVYWAGPLIGGGIAGLVYEVLF (213–235)
Outward-rectifier K^+ channel TOK1 (P40310)	HWFSLSVTIAIFMAFWLLGALVF (377–399)
TrpC1 (O18784)	HSFIGTCFALFWYIFSLAHVAIL (584–606)
TrpC5 (Q9UL62)	HTASYLTFLFMLLLASQHIV (369–388)
Acid-activated urea channel (P56874)	HLTSFYGPATGLLFGFTYLYAAI (70–92)
L-type Ca^{2+} channel (Q02789)	HISDILNVAFTIIFTLEMVLKLI (1147–1169)

The Swiss-Prot database was searched for proteins annotated as channels. In these proteins, the transmembrane domains were predicted with TMHMM (Sonnhammer et al., 1998). Note that some of the proteins are known to be influenced by pH (e.g. O14649, P56874, and P56874). The Swiss-Prot name is listed in parentheses.

simulations, the peptides were N-terminally acetylated and C-terminally methyl-amidated. Six different systems were constructed with different protonation states of the histidines residues, as shown in Figure 1.

Simulation System

The membrane environment in which the simulation took place was constructed by using a preequilibrated lipid bilayer initially made up of 128 dimyristoylphosphocholine lipids embedded in 3687 molecules of SPC water (Berendsen et al., 1981). In order to insert the protein into the dimyristoylphosphocholine bilayer, a hole was generated, as described in detail in Faraldo-Gomez et al. (2002). Na^+ counterions were added to neutralize the system charge according to the protonation state of the channel. They replaced water molecules at positions corresponding to the lowest Coulombic energy of the ions.

Simulation Stages

The protein-bilayer-solvent systems were energy minimized, followed by equilibration in two stages. First, the system underwent 0.5 ns of an MD run with positional restraints on the protein. In all other molecules, all bond lengths and angles were constrained. Second, the system underwent 0.5 ns of an MD run with positional restraints on the protein atoms, so as to improve the packing of lipids around the protein. Thereafter, the equilibrated systems were subjected to a 7.5 ns MD simulation.

Simulation Details

The simulations were conducted by using version 3.2.1 of the GROMACS MD simulation package (Lindahl et al., 2001) employing an extended version of the GROMOS87 force field (Hermans et al., 1984). Dimyristoylphosphocholine force field parameters were taken from Berger et al. (1997). All simulations were conducted by using the LINCS algorithm (Hess et al., 1997) to constrain bond lengths and angles of hydrogen atoms, allowing a time step of 2 fs. Atomic coordinates were saved every 0.5 ps. Simulations were conducted at a constant temperature of 310 K. Solvent, lipid, and protein were coupled separately to a Nose-Hoover temperature bath (Nose, 1984; Hoover, 1985), with a coupling constant of $\tau = 3$ ps. The pressure was kept constant by anisotropic coupling of the system to a Parrinello-Rahman pressure bath (Parrinello and Rahman, 1981; Nose and Klein, 1983) of 1 bar, with a coupling constant of $\tau = 3$ ps. A cutoff of 1 nm was used for van der Waals interactions. Electrostatic interactions were computed by using the PME algorithm (Darden et al., 1993), with a 1 nm cutoff for the direct space calculation. The partial charges for the protein, water, and ions atoms were taken from the GROMOS87 force field (Hermans et al., 1984). Parameters of dimyristoylphosphocholine atoms were adopted from Berger et al. (1997). The partial charges of the two different protonation states of the histidine residues involve explicit charge delocalization. Moreover, the histidine's side chain has no net charge when not protonated, while, in the protonated state, it has a positive charge at the magnitude of 1.08.

pKa Calculations

The pKa of transitions between different protonation states was calculated by solving the Poisson-Boltzmann equation on a grid (Warwicker and Watson, 1982), by using the program MEAD (Bashford and Gerwert, 1992). This program solves the linearized Poisson-Boltzmann equation for molecular systems by a finite difference method (Warwicker and Watson, 1982). The inner and outer dielectric constants applied to the model and the solvent were fixed at 4.0

and 80.0, respectively. In order to solve the Poisson-Boltzmann equation, we performed grid focusing in two steps. Initially, we used a cube with a 1.0 Å lattice spacing centered at the geometric center of the model, followed by a cube with a 0.25 Å lattice spacing centered at the histidine residues of interest. The model pK for the histidine residues was chosen to be 6.7. The structures used in the pKa calculation consisted of the averaged structures, in which a H^+ was removed from the histidine residues of interest.

Acknowledgments

The authors wish to thank H. Leonov, E.R. Bennett, and E. Arbely for the helpful discussions, as well as D. Bashford for help with running the pKa calculations. This research was supported in part by grants from the Israel Science Foundation (784/01), Deutsche Forschungsgemeinschaft (SA 7772/6-1), and from Niedersachsen to I.T.A.

Received: March 23, 2005
Revised: July 14, 2005
Accepted: August 14, 2005
Published: December 13, 2005

References

Arbely, E., Khattari, Z., Brotons, G., Akkawi, M., Salditt, T., and Arkin, I.T. (2004). A highly unusual palindromic transmembrane helical hairpin formed by SARS coronavirus E protein. J. Mol. Biol. *341*, 769–779.

Bashford, D., and Gerwert, K. (1992). Electrostatic calculations of the pKa values of ionizable groups in bacteriorhodopsin. J. Mol. Biol. *224*, 473–486.

Berendsen, H.J.C., Postma, J.P.M., van Gunsteren, W.F., and Hermans, J. (1981). Interaction models for water in relation to protein hydration. In Intermolecular Forces, B. Pullman, ed. (Dordrecht: The Netherlands: D. Reidel Publishing Company), pp. 331–342.

Berger, O., Edholm, O., and Jahnig, F. (1997). Molecular dynamics simulations of a fluid bilayer of dipalmitoylphosphatidylcholine at full hydration, constant pressure, and constant temperature. Biophys. J. *72*, 2002–2013.

Brewer, M.L., Schmitt, U.W., and Voth, G.A. (2001). The formation and dynamics of proton wires in channel environments. Biophys. J. *80*, 1691–1702.

Chanchevalap, S., Yang, Z., Cui, N., Qu, Z., Zhu, G., Liu, C., Giwa, L.R., Abdulkadir, L., and Jiang, C. (2000). Involvement of histidine residues in proton sensing of ROMK1 channel. J. Biol. Chem. *275*, 7811–7817.

Chizhmakov, I.V., Geraghty, F.M., Ogden, D.C., Hayhurst, A., Antoniou, M., and Hay, A.J. (1996). Selective proton permeability and pH regulation of the influenza virus M2 channel expressed in mouse erythroleukaemia cells. J. Physiol. *494*, 329–336.

Chizhmakov, I.V., Ogden, D.C., Geraghty, F.M., Hayhurst, A., Skinner, A., Betakova, T., and Hay, A.J. (2003). Differences in conductance of M2 proton channels of two influenza viruses at low and high pH. J. Physiol. *546*, 427–438.

Darden, T., York, D., and Pedersen, L. (1993). Particle mesh Ewald: an N-log(N) method for Ewald sums in large systems. J. Chem. Phys. *98*, 10089–10092.

de Groot, B.L., and Grubmuller, H. (2001). Water permeation across biological membranes: mechanism and dynamics of aquaporin-1 and GlpF. Science *294*, 2353–2357.

Duff, K.C., and Ashley, R.H. (1992). The transmembrane domain of influenza A M2 protein forms amantadine-sensitive proton channels in planar lipid bilayers. Virology *190*, 485–489.

Duff, K.C., Kelly, S.M., Price, N.C., and Bradshaw, J.P. (1992). The secondary structure of influenza A M2 transmembrane domain. A circular dichroism study. FEBS Lett. *311*, 256–258.

Duong-Ly, K.C., Nanda, V., Degrado, W.F., and Howard, K.P. (2005). The conformation of the pore region of the M2 proton channel depends on lipid bilayer environment. Protein Sci. *14*, 856–861.

Faraldo-Gomez, J.D., Smith, G.R., and Sansom, M.S. (2002). Setting up and optimization of membrane protein simulations. Eur. Biophys. J. *31*, 217–227.

Forrest, L.R., Kukol, A., Arkin, I.T., Tieleman, D.P., and Sansom, M.S. (2000). Exploring models of the influenza A M2 channel: MD simulations in a phospholipid bilayer. Biophys. J. *78*, 55–69.

Hay, A.J., Wolstenholme, A.J., Skehel, J.J., and Smith, M.H. (1985). The molecular basis of the specific anti-influenza action of amantadine. EMBO J. *4*, 3021–3024.

Hermans, J., Berendsen, H.J.C., van Gunsteren, W.F., and Postma, J.P.M. (1984). A consistent empirical potential for water-protein interactions. Biopolymers *23*, 1513–1518.

Hess, B., Bekker, H., Berendsen, H.J.C., and Fraaije, J.G.E.M. (1997). LINCS: a linear constraint solver for molecular simulations. J. Comp. Chem. *18*, 1463–1472.

Holsinger, L.J., Shaughnessy, M.A., Micko, A., Pinto, L.H., and Lamb, R.A. (1995). Analysis of the posttranslational modifications of the influenza virus M2 protein. J. Virol. *69*, 1219–1225.

Hoover, W. (1985). Canonical dynamics - equilibrium phase-space distributions. Phys. Rev. A. *31*, 1695–1697.

Humphrey, W., Dalke, A., and Schulten, K. (1996). VMD: visual molecular dynamics. J. Mol. Graph. *14*, 33–38.

Husslein, T., Moore, P.B., Zhong, Q., Newns, D.M., Pattnaik, P.C., and Klein, M.L. (1998). Molecular dynamics simulation of a hydrated diphytanol phosphatidylcholine lipid bilayer containing an α-helical bundle of four transmembrane domains of the influenza A virus M2 protein. Faraday Discuss. *111*, 201–208.

Kim, S., Chamberlain, A.K., and Bowie, J.U. (2003). A simple method for modeling transmembrane helix oligomers. J. Mol. Biol. *329*, 831–840.

Kovacs, F.A., and Cross, T.A. (1997). Transmembrane four-helix bundle of influenza A M2 protein channel: structural implications from helix tilt and orientation. Biophys. J. *73*, 2511–2517.

Kovacs, F.A., Denny, J.K., Song, Z., Quine, J.R., and Cross, T.A. (2000). Helix tilt of the M2 transmembrane peptide from influenza A virus: an intrinsic property. J. Mol. Biol. *295*, 117–125.

Kukol, A., Adams, P.D., Rice, L.M., Brunger, A.T., and Arkin, T.I. (1999). Experimentally based orientational refinement of membrane protein models: a structure for the Influenza A M2 H+ channel. J. Mol. Biol. *286*, 951–962.

Lear, J.D. (2003). Proton conduction through the M2 protein of the influenza A virus; a quantitative, mechanistic analysis of experimental data. FEBS Lett. *552*, 17–22.

Lin, T.I., and Schroeder, C. (2001). Definitive assignment of proton selectivity and attoampere unitary current to the M2 ion channel protein of influenza A virus. J. Virol. *75*, 3647–3656.

Lindahl, E., Hess, B., and van der Spoel, D. (2001). GROMACS 3.0: a package for molecular simulation and trajectory analysis. J. Mol. Mod. *7*, 306–317.

Lindskog, S. (1997). Structure and mechanism of carbonic anhydrase. Pharmacol. Ther. *74*, 1–20.

Mould, J.A., Paterson, R.G., Takeda, M., Ohigashi, Y., Venkataraman, P., Lamb, R.A., and Pinto, L.H. (2003). Influenza B virus BM2 protein has ion channel activity that conducts protons across membranes. Dev. Cell *5*, 175–184.

Nishimura, K., Kim, S., Zhang, L., and Cross, T.A. (2002). The closed state of a H+ channel helical bundle combining precise orientational and distance restraints from solid state NMR. Biochemistry *41*, 13170–13177.

Nose, S. (1984). A molecular-dynamics method for simulations in the canonical ensemble. Mol. Phys. *52*, 255–268.

Nose, S., and Klein, M. (1983). Constant pressure molecular-dynamics for molecular-systems. Mol. Phys. *50*, 1055–1076.

Noskov, S.Y., Berneche, S., and Roux, B. (2004). Control of ion selectivity in potassium channels by electrostatic and dynamic properties of carbonyl ligands. Nature *431*, 830–834.

Okada, A., Miura, T., and Takeuchi, H. (2001). Protonation of histidine and histidine-tryptophan interaction in the activation of the M2 ion channel from influenza a virus. Biochemistry *40*, 6053–6060.

Padanilam, B.J., Lu, T., Hoshi, T., Padanilam, B.A., Shibata, E.F., and Lee, H.C. (2002). Molecular determinants of intracellular pH modulation of human Kv1.4 N-type inactivation. Mol. Pharmacol. *62*, 127–134.

Parrinello, M., and Rahman, A. (1981). Polymorphic transitions in single crystals: a new molecular dynamics method. J. Appl. Phys. *52*, 7182–7190.

Persistence of Vision Raytracer Pty. Ltd. (2004). Persistence of Vision Raytracer (Version 3.6) (http://www.povray.org/).

Pinto, L.H., Holsinger, L.J., and Lamb, R.A. (1992). Influenza virus M2 protein has ion channel activity. Cell *69*, 517–528.

Pinto, L.H., Dieckmann, G.R., Gandhi, C.S., Papworth, C.G., Braman, J., Shaughnessy, M.A., Lear, J.D., Lamb, R.A., and DeGrado, W.F. (1997). A functionally defined model for the M2 proton channel of influenza A virus suggests a mechanism for its ion selectivity. Proc. Natl. Acad. Sci. USA *94*, 11301–11306.

Sakaguchi, T., Tu, Q., Pinto, L.H., and Lamb, R.A. (1997). The active oligomeric state of the minimalistic influenza virus M2 ion channel is a tetramer. Proc. Natl. Acad. Sci. USA *94*, 5000–5005.

Sansom, M.S.P., Kerr, I.D., Smith, G.R., and Son, H.S. (1997). The influenza A virus M2 channel: a molecular modeling and simulation study. Virology *233*, 163–173.

Sansom, M.S., Tieleman, D.P., Forrest, L.R., and Berendsen, H.J. (1998). Molecular dynamics simulations of membranes with embedded proteins and peptides: porin, alamethicin and influenza virus M2. Biochem. Soc. Trans. *26*, 438–443.

Schmitt, U., and Voth, G. (1998). Multistate empirical valence bond model for proton transport in water. J. Phys. Chem. B *102*, 5547–5551.

Schmitt, U., and Voth, G. (1999a). Quantum properties of the excess proton in liquid water. Isr. J. Chem. *39*, 483–492.

Schmitt, U.W., and Voth, G.A. (1999b). The computer simulation of proton transport in water. J. Phys. Chem. *111*, 9361–9381.

Smart, O.S., Neduvelil, J.G., Wang, X., Wallace, B.A., and Sansom, M.S. (1996). HOLE: a program for the analysis of the pore dimensions of ion channel structural models. J. Mol. Graph. *14*, 354–360.

Smondyrev, A.M., and Voth, G.A. (2002). Molecular dynamics simulation of proton transport through the influenza A virus M2 channel. Biophys. J. *83*, 1987–1996.

Song, Z., Kovacs, F.A., Wang, J., Denny, J.K., Shekar, S.C., Quine, J.R., and Cross, T.A. (2000). Transmembrane domain of M2 protein from influenza A virus studied by solid-state (15)N polarization inversion spin exchange at magic angle NMR. Biophys. J. *79*, 767–775.

Sonnhammer, E.L., von Heijne, G., and Krogh, A. (1998). A hidden Markov model for predicting transmembrane helices in protein sequences. Proc. Int. Conf. Intell. Syst. Mol. Biol. *6*, 175–182.

Sugrue, R.J., and Hay, A.J. (1991). Structural characteristics of the M2 protein of influenza A viruses: evidence that it forms a tetrameric channel. Virology *180*, 617–624.

Tajkhorshid, E., Nollert, P., Jensen, M.O., Miercke, L.J., O'Connell, J., Stroud, R.M., and Schulten, K. (2002). Control of the selectivity of the aquaporin water channel family by global orientational tuning. Science *296*, 525–530.

Takeuchi, H., Okada, A., and Miura, T. (2003). Roles of the histidine and tryptophan side chains in the M2 proton channel from influenza A virus. FEBS Lett. *552*, 35–38.

Torres, J., and Arkin, I.T. (2002). C-deuterated alanine: a new label to study membrane protein structure using site-specific infrared dichroism. Biophys. J. *82*, 1068–1075.

Torres, J., Kukol, A., and Arkin, I.T. (2000). Use of a single glycine residue to determine the tilt and orientation of a transmembrane helix. A new structural label for infrared spectroscopy. Biophys. J. *79*, 3139–3143.

Torres, J., Kukol, A., Goodman, J.M., and Arkin, I.T. (2001). Site-specific examination of secondary structure and orientation determination in membrane proteins: the peptidic (13)C=(18)O group as a novel infrared probe. Biopolymers *59*, 396–401.

Vijayvergiya, V., Wilson, R., Chorak, A., Gao, P.F., Cross, T.A., and Busath, D.D. (2004). Proton conductance of influenza virus M2 protein in planar lipid bilayers. Biophys. J. *87*, 1697–1704.

Wang, C., Lamb, R.A., and Pinto, L.H. (1995). Activation of the M2 ion channel of influenza virus: a role for the transmembrane domain histidine residue. Biophys. J. *69*, 1363–1371.

Wang, J., Kim, S., Kovacs, F., and Cross, T.A. (2001). Structure of the transmembrane region of the M2 protein H(+) channel. Protein Sci. *10*, 2241–2250.

Warwicker, J., and Watson, H.C. (1982). Calculation of the electric potential in the active site cleft due to alpha-helix dipoles. J. Mol. Biol. *157*, 671–679.

Xu, H., Wu, J., Cui, N., Abdulkadir, L., Wang, R., Mao, J., Giwa, L.R., Chanchevalap, S., and Jiang, C. (2001). Distinct histidine residues control the acid-induced activation and inhibition of the cloned K(ATP) channel. J. Biol. Chem. *276*, 38690–38696.

Zhong, Q., Husslein, T., Moore, P.B., Newns, D.M., Pattnaik, P., and Klein, M.L. (1998). The M2 channel of influenza A virus: a molecular dynamics study. FEBS Lett. *434*, 265–271.

Zhong, Q., Newns, D.M., Pattnaik, P., Lear, J.D., and Klein, M.L. (2000). Two possible conducting states of the influenza A virus M2 ion channel. FEBS Lett. *473*, 195–198.